Pergamon

Int. J. Heat Mass Transfer. Vol. 37, No. 10, pp. 1465–1473, 1994

0017–9310/94 \$7.00+0.00

0017-9310(93)0097-Z

Developing flow and heat transfer in radially rotating rectangular ducts with wall-transpiration effects

WEI-MON YAN

Department of Mechanical Engineering, Hua Fan College of Humanities and Technology, Shih Ting, Taipei, Taiwan 22305, R.O.C.

(*Received* 4 *August* 1993 *and in final form* 17 *November* 1993)

Abstract—A numerical study is made to investigate the characteristics of heat transfer and fluid flow in radially rotating rectangular ducts with wall-transpiration effects. The predicted results are presented for air flowing in an isothermal rectangular duct over a wide range of the governing parameters. In this work, the wall Reynolds numbers, Re_w, are varied from 0 to 20 with rotation numbers, Ro, ranging from 0 to 0.1. The inlet Reynolds numbers, Re, are varied from 500 to 2000 for aspect ratios $\gamma = 0.2$, 0.5, 1, 2, and 5. The axial variations of the averaged fRe and Nu are characterized by a decay near the entrance due to the entrance effect; but the decay is attenuated by the onset of secondary flow due to the combined effects of Coriolis force and wall suction. The averaged Nu is enhanced with an increase in the wall Reynolds number, Re_w, rotation number, Ro, or inlet Reynolds number, Re. Additionally, the predicted fRe shows that, near the entrance, the fRe increases with Re_w. But as the flow moves downstream, the fRe decreases with Re_w.

INTRODUCTION

THE HEAT transfer and fluid flow in porous-walled passages have received great attention in the past decades due to their wide applications in a variety of thermal systems. The porous-walled ducts are used in the transpiration cooling of high temperature thermal systems, gas-turbine blades, combustion chambers, exhaust nozzles, porous-walled flow reactors and solar energy collectors. Among these, the transpiration cooling of rotating turbine blades is to prevent the blade failure due to the combination of high thermal loads and centrifugal stressing. Considering the orientation of flow passage and the axis of rotation, there are five rotation modes: radial or orthogonal mode, parallel mode, axial mode, slant mode and circumferential mode. Among these five modes, the radial mode is the most interesting one for its application to rotor blade cooling in gas turbines. Flow and heat transfer mechanisms in a radially rotating channel are very complicated due to the presence of Coriolis-induced secondary flow.

In an engineering point of view, the transpiration cooling in turbine rotor blades can be modeled as the heat convection in radially rotating ducts with wall-transpiration [1, 2]. The coolant air flows through the coolant passage and transpires out through the porous skin. As explained by Hennecks [1], the transpiration cooling is the most efficient means for thermal protection of the turbine blades. The high efficiency stems from two mechanisms: (1) the heat is carried away by the coolant air through the duct, and (2) the relatively cool (compared to the external hot gas stream) fluid transpired through the porous skin forms a high thermal-resistance protection layer over the blade.

The effects of Coriolis force on the flow fields in unheated, rotating ducts have been studied in many investigations, e.g. the theoretical and experimental works by Hart [3], Ito and Nanbu [4], Wagner and Velkoff [5], Moore [6, 7], Majumdar and Spalding [8], Majumdar *et al.* [9], Speziale [10, 11], and Speziale and Thangam [12]. These investigators have documented the presence of Coriolis-induced secondary flow. The studies of flow and heat transfer in rotating ducts were conducted by Mori *et al.* [13], Vidyanidhi *et al.* [14], Metzger and Stan [15], Morris and Ayhan [16, 17], Clifford *et al.* [18], Hwang and Soong [19], Hwang and Jen [20], Wagner *et al.* [21, 22], Soong *et al.* [23], Fann *et al.* [24], Fann and Yang [25], Han and Zhang [26], Jen *et al.* [27] and Jen and Lavine [28]. Some investigators found that large increase and decrease in trailing and leading surface heat transfer occurred under certain conditions of rotation while others showed lesser effects. The inconsistencies exist between investigators due to differences in the measurement techniques, models and test conditions [21, 22]. In these studies, no wall-transpiration effects are included.

Fully-developed flows in the stationary duct with wall transpiration have been investigated by Wageman and Guevana [29], Hornbeck *et al.* [30], Prager [31], Terrill and Thomas [32], Terrill [33, 34], and Idel'chik and Shteinberg [35]. Studies on developing flows in porous-walled ducts with suction and injection effects were performed by Raithby and Knudsen

NOMENCLATURE

A	cross-sectional area of a rectangular duct [m^2]
a, b	width and height of a rectangular duct, respectively [m]
D_e	equivalent hydraulic diameter, $4A/S$
f	friction factor, $2\bar{\tau}_w/(\rho \bar{w}_o^2)$
$\bar{h}$	circumferentially averaged heat transfer coefficient [W m^{-2} °C^{-1}]
h_x	locally averaged heat transfer coefficient [W m^{-2} °C^{-1}]
I, J	number of finite difference divisions in X and Y directions, respectively
m	mth iteration
n	dimensionless direction coordinate normal to the duct wall
Nu	peripherally averaged Nusselt number, $\bar{h}D_e/k$
Nu_x	locally averaged Nusselt number, $h_x D_e/k$
p	pressure [kPa]
p_m	dynamic pressure [kPa]
$\bar{p}$, $\bar{P}$	pressure and dimensionless pressure averaged over a cross section
P'	perturbation term about the mean pressure $\bar{P}$
Pr	Prandtl number, ν/α
Re	inlet Reynolds number of the gas stream, $\bar{w}_o D_e/\nu$
Re_w	wall Reynolds number, $u_w D_e/\nu$
Ro	rotation number, $\Omega D_e/\bar{w}_o$
S	circumference of cross section [m]
T	temperature [°C]
T_o	inlet temperature [°C]
T_w	wall temperature [°C]
u, v, w	velocity components in x, y and z directions, respectively [m s^{-1}]
U, V, W	dimensionless velocity components in x, y and z directions, respectively
U_w	suction velocity at porous wall, $u_w/\bar{w}_o$
$\bar{w}$	local mean velocity in axial direction [m s^{-1}]
$\bar{w}_o$	mean velocity at inlet [m s^{-1}]
x, y, z	rectangular coordinates [m]
X, Y, Z	dimensionless rectangular coordinates, $X = x/D_e$, $Y = y/D_e$, $Z = z/D_e$.

Greek symbols

α	thermal diffusivity [m^2 s^{-1}]
γ	aspect ratio of a rectangular duct, a/b
θ	dimensionless temperature, $(T-T_o)/(T_w-T_o)$
ν	kinematic viscosity [m^2 s^{-1}]
ξ	dimensionless vorticity in axial direction
ρ	density [kg m^{-3}]
τ_w	wall shear stress [kPa]
Ω	angular velocity of rotation [s^{-1}].

Subscripts

b	bulk fluid quantity
o	condition at inlet
w	value at wall.

Superscript

—	averaged value.

[36], Sorour *et al.* [37], Tsai and Liou [38, 39]. The effects of mass extraction and injection on the fully-developed heat convection were also examined by the asymptotic analysis [40] and numerical calculation [41]. In the former, buoyancy effects were considered in the porous channel as well as the porous tube, but the results were limited to the small transpiration rates. While in the latter, only forced convection in the porous walled tube was studied. The thermal entrance heat transfer with fully-developed velocity distributions in porous ducts was carried out by Pederson and Kinney [42] and Raithby [43]. In refs. [42, 43], various thermal boundary conditions were investigated. The numerical analyses for the simultaneously developing flow and temperature fields in the entrance region of porous ducts were examined by Doughty and Perkins [44, 45], Rhee and Edwards [46] and Fagher [47]. They found that the wall-transpiration has a significant impact on the heat transfer and fluid flow in the entrance region of porous ducts.

It is noted that, in the above review, study of flow and heat transfer in rotating ducts with wall transpiration has not received sufficient attention. Recently, Soong and Hwang [48, 49] solved the flow and heat transfer in two-dimensional semiporous-walled channel in the presence of rotation by the similarity method. In their studies, the height/width aspect ratio was assumed to be small in order to neglect the side effect. From an engineering point of view, only ducts with very small height/width aspect ratios can be treated as parallel plates. Also, many applications are known to have a moderate or high aspect aspect ratio. This motivates the present study which is to examine the fluid flow and heat transfer in rotating rectangular ducts with wall-transpiration. Both flow and heat transfer characteristics in developing laminar flow are studied numerically.

ANALYSIS

Consider the steady and laminar flow through an isothermal rectangular duct rotating at a constant

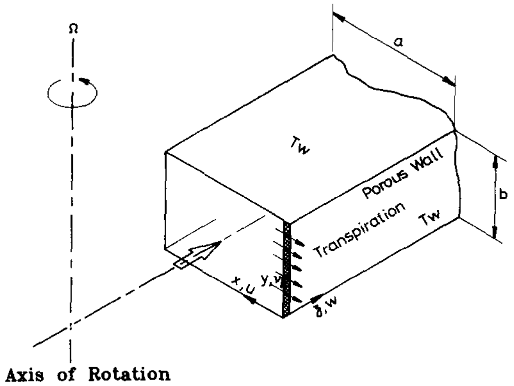

FIG 1. Schematic diagram of the physical system.

angular speed Ω about an axis normal to the longitudinal direction of the duct as shown in Fig. 1. The flow is subjected to a uniform suction from the porous wall. The suction fluid is the same as that of the duct flow and has the same temperature of the heated wall. A uniform inlet axial velocity $\bar{w}_o$ and a constant inlet temperature T_o are imposed at the entrance $z = 0$. The duct walls are held at constant temperature at T_w. The u, v and w are the velocity components in the x, y and z directions, respectively. The flow is assumed to be steady and of constant property. Furthermore, to facilitate the analysis, the axial diffusion, viscous dissipation, compression work, and buoyancy are neglected. It is worth noting that centrifugal-buoyancy may not be neglected as the rotational rate is large [27, 28]. Therefore, the present calculations will cover the low to moderate rotational rates at which the centrifugal-buoyancy effect is relatively small. Note that, once centrifugal-buoyancy is ignored, the distance from the axis of rotation to the duct inlet is irrelevant.

Governing equations

The pressure gradient and centrifugal force terms in the x- and z-directions are:

$$-\partial p/\partial x+\rho\Omega^2 x \tag{1a}$$

$$-\partial p/\partial z+\rho\Omega^2(z_o+z). \tag{1b}$$

With a dynamic pressure p_m defined as

$$p_m = p-p_o \tag{2}$$

where

$$-\partial p_o/\partial x = -\rho_o\Omega^2 x \tag{3a}$$

$$-\partial p_o/\partial z = -\rho_o\Omega^2(z_o+z) \tag{3b}$$

equation (1) may be rewritten as

$$-\partial p/\partial x+\rho\Omega^2 x = -\partial p_m/\partial x \tag{4a}$$

$$-\partial p/\partial z+\rho\Omega^2(z_o+z) = -\partial p_m/\partial z. \tag{4b}$$

The flow is assumed to be parabolic and, in the momentum equations, a space-averaged pressure $\bar{p}$ is imposed to prevail at each cross-section and, therefore, to permit a decoupling from the pressure p_m in the cross-sectional momentum equations. This 'pressure uncoupling' follows the parabolic-flow practice and, together with the assumption that neither momentum nor heat is diffused in the axial direction by an order of analysis, permits a marching-integration calculation procedure [27, 50]. To conveniently present the governing equations, the dynamic pressure p_m can be represented as the sum of a cross-section mean pressure $\bar{p}(z)$, which derives the main flow, and a perturbation about the mean, $p'(x,y)$, which derives the cross stream flow,

$$p_m = \bar{p}(z)+p'(x,y). \tag{5}$$

Referring to the coordinate system shown in Fig. 1 and introducing the following dimensionless variables and parameters,

$$\begin{gathered} X = x/D_e \quad Y = y/D_e \quad Z = z/D_e \quad U = u/\bar{w}_o \\ V = v/\bar{w}_o \quad W = w/\bar{w}_o \\ \bar{P} = \bar{p}/(\rho\bar{w}_o^2) \quad P' = p'/(\rho\bar{w}_o^2) \\ \theta = (T-T_o)/(T_w-T_o) \quad U_w = u_w/\bar{w}_o \\ Re_w = u_w D_e/\nu \quad Ro = \Omega D_e/\bar{w}_o \\ Re = \bar{w}_o D_e/\nu \quad Pr = \nu/\alpha \quad \gamma = a/b \quad D_e = 4A/S \end{gathered} \tag{6}$$

the following dimensionless vorticity–velocity formulation of governing equations can be obtained [25, 27]:

$$\partial^2 U/\partial X^2+\partial^2 U/\partial Y^2 = \partial\xi/\partial Y-\partial^2 W/\partial X\partial Z \tag{7}$$

$$\partial^2 V/\partial X^2+\partial^2 V/\partial Y^2 = -\partial\xi/\partial X-\partial^2 W/\partial Y\partial Z \tag{8}$$

$$\begin{aligned} &U\partial\xi/\partial X+V\partial\xi/\partial Y+W\partial\xi/\partial Z \\ &\quad+\xi(\partial U/\partial X+\partial V/\partial Y)+(\partial W/\partial Y.\partial U/\partial Z \\ &\quad-\partial W/\partial X.\partial V/\partial Z)+2Ro\cdot\partial W/\partial Y \\ &\qquad= (\partial^2\xi/\partial X^2+\partial^2\xi/\partial Y^2)/Re \end{aligned} \tag{9}$$

$$\begin{aligned} &U\partial W/\partial X+V\partial W/\partial Y+W\partial W/\partial Z \\ &\quad= -\mathrm{d}\bar{P}/\mathrm{d}Z+(\partial^2 W/\partial X^2+\partial^2 W/\partial Y^2)/Re+2Ro\cdot U \end{aligned} \tag{10}$$

$$\begin{aligned} &U\partial\theta/\partial X+V\partial\theta/\partial Y+W\partial\theta/\partial Z \\ &\quad= (\partial^2\theta/\partial X^2+\partial^2\theta/\partial Y^2)/(Pr\cdot Re) \end{aligned} \tag{11}$$

where $\xi = \partial U/\partial Y-\partial V/\partial X$ is the axial vorticity.

Equations (7)–(10) are used for solving U, V, W and ξ. An additional constraint for deduction of the pressure gradient in the axial momentum equation can be derived from the overall mass balance at every axial location. This can be expressed as

$$\bar{W} = 1-(Re_w/Re)\,[2/(1+\gamma)]Z. \tag{12}$$

In summary, the governing equations for the flow include: (i) the axial momentum equation (10), (ii) the axial vorticity equation (9) and the transverse velocity components (7) and (8). They are of parabolic–elliptic form. This formulation is called the velocity–vorticity method [51]. Flow temperature is determined by equation (11).

The boundary conditions for this problem are given by

$$W = 1, U = V = \xi = \theta = 0 \text{ at the entrance } Z = 0 \quad (13a)$$

$$U = V = W = 0, \theta = 1 \text{ on the solid walls} \quad (13b)$$

$$U = U_w = -Re_w/Re, V = W = 0, \theta = 1 \text{ on the porous wall.} \quad (13c)$$

After the developing velocity and temperature fields are obtained, the computations of the circumferentially averaged friction factor and Nusselt number are of practical interest. Following the usual definition, the expression for the product of the peripherally averaged friction factor and Reynolds number, fRe, can be written based on the axial velocity gradient on the duct wall:

$$fRe = 2(\overline{\partial W/\partial n})_w. \quad (14)$$

By using the temperature gradient on the duct walls, the peripherally averaged Nusselt number, Nu, is expressed as:

$$Nu = -(\overline{\partial\theta_w/\partial n})/(1-\theta_b) \quad (15)$$

where the overbar means average around the perimeter and n denotes the dimensionless coordinate normal to the duct wall. The bulk temperature θ_b is defined as

$$\theta_b = \int_0^{(1+\gamma)/(2\gamma)} \int_0^{(1+\gamma)/2} \theta \cdot W \mathrm{d}X\mathrm{d}Y \Big/ \int_0^{(1+\gamma)/(2\gamma)} \int_0^{(1+\gamma)/2} W \mathrm{d}X\mathrm{d}Y. \quad (16)$$

Governing parameters

The parameters involved in the present problem are the Prandtl number, Pr, wall Reynolds number, Re_w, rotation number, Ro, inlet Reynolds number of the gas stream, Re, and cross-sectional aspect ratio, γ. The rotation number, Ro, represents the relative importance of the Coriolis force to the inertia force or the relative significance of the Coriolis-induced secondary flow to the forced flow effects. The Re_w measures the importance of the wall-transpiration effects. The ranges of the parameters for the present study are wall Reynolds numbers $Re_w = 0, 5, 10, 15$ and 20; rotation numbers $Ro = 0, 0.025, 0.05, 0.075$ and 0.1; Reynolds numbers $Re = 500, 1000, 1500$ and 2000; aspect ratios $\gamma = 0.2, 0.5, 1.0, 2.0$ and 5.0; and Prandtl number $Pr = 0.7$ (air).

SOLUTION METHOD

The governing equations are numerically solved by the vorticity–velocity method for three-dimensional parabolic flow [51]. The equations for the unknowns U, V, W, ξ and $\mathrm{d}\bar{P}/\mathrm{d}Z$ are coupled. A numerical finite-difference scheme based on the vorticity velocity method is used to obtain the solution of equations (7)–(11). The solution procedures are as follows.

(1) Assign initial values for the velocity components and temperature difference, $U = V = \theta = \xi = 0$ and $W = 1$ at the entrance.

(2) With the known values of U, V and assigned $(\mathrm{d}\bar{P}/\mathrm{d}Z)$, find new values of W and ξ at interior points of the next axial position from equations (10) and (9), respectively, by the Du Fort–Frankel method [52].

(3) Check the satisfaction of the averaged axial velocity $\bar{W}$, equation (12). If not, guess a new $(\mathrm{d}\bar{P}/\mathrm{d}Z)$ by the Newton–Raphson method and repeat steps (2) and (3).

(4) The values of $\partial^2 W/\partial X\,\partial Z$, $\partial^2 W/\partial Y\,\partial Z$, $\partial\xi/\partial Y$, and $\partial\xi/\partial X$ in equations (7) and (8) are calculated by using backward difference axially and central difference in the transverse directions. The elliptic-type equations (7) and (8) are then solved for U and V by iteration. During iteration process, values of vorticity on boundaries are evaluated simultaneously with U and V in the interior region. These boundary vorticities on the four walls can be evaluated with the expressions given by Chou and Hwang [53].

(5) Step (4) is repeated at a cross section until the following criterion is satisfied for the velocity components U and V,

$$\varepsilon = \mathrm{Max}|\phi_{i,j}^{m+1} - \phi_{i,j}^{m}|/\mathrm{Max}|\phi_{i,j}^{m+1}| < 10^{-5}, \quad \phi = U \text{ or } V \quad (17)$$

where m is the mth iteration of step (4).

(6) Obtain new values of θ at the next axial location from equation (11) by the Du Fort–Frankel method.

(7) Steps (2)–(6) are repeated at each axial location from the entrance to the downstream of interest.

To obtain enhanced accuracy, grids were chosen to be uniform in the cross-sectional direction but non-uniform in the axial direction to account for the uneven variations of velocity and temperature in the entrance region. A numerical experiment for the case of $Re_w = 10$, $Ro = 0.05$, $Re = 1500$, and $\gamma = 1$ was made to determine the grid spacing and axial step size required for acceptable accuracy. As shown in Table 1, the deviations in Nu calculated with either $I \times J = 35\times35$ or 45×45 $(\Delta Z = 0.01 \sim 0.05)$ are always within 3%. Furthermore, the deviations in Nu calculated using either $I \times J$ $(\Delta Z) = 35\times35$ $(0.002 \sim 0.05)$ or 35×35 $(0.01 \sim 0.05)$ are all less than 1%. Accordingly, the computations involving an $I\times J\,(\Delta Z) = 35\times35\,(0.01 \sim 0.05)$ grid are considered to be sufficiently accurate to describe the flow and heat transfer in a radially rotating rectangular duct with wall-transpiration. All the results presented in the next section are computed using the latter grid.

As a partial verification of the computational procedure, results were initially obtained for laminar convection heat transfer in a radially rotating rectangular

Table 1. Comparisons of averaged Nusselt number Nu for various grid arrangements with $Re_w = 10$, $Ro = 0.05$, $Re = 1500$, and $\gamma = 1$

$I \times J$ (ΔZ)	Z					
	2.503	5.005	10.018	20.043	30.018	40.0
45×45 ($0.01 \sim 0.05$)	9.869	8.761	9.724	11.625	13.037	13.792
35×35 ($0.002 \sim 0.05$)	10.027	8.974	10.042	11.927	13.327	14.157
35×35 ($0.01 \sim 0.05$)	10.0	8.970	10.040	11.933	13.330	14.158
25×25 ($0.01 \sim 0.05$)	10.548	9.575	11.135	13.208	14.748	15.709

duct without wall-transpiration effect. The results for heat transfer and friction factor were compared with those by Fann and Yang [25] and Jen *et al.* [27]. The Nusselt number and friction factor were found to agree within 2%. In addition, the hydrodynamically developing flow without rotation was calculated. These results are compared with Shah and London [54]. As shown in Table 2, the differences in the fanning friction factor are within 1% at all axial locations. The above numerical tests indicate that the solution procedure adopted is suitable for the present study.

RESULTS AND DISCUSSION

The developing axial velocity profiles along the centerline $Y = 0.5$ are depicted in Fig. 2 at various axial locations. It is well known that the axial velocity profiles for purely forced convection without rotation effect are symmetric with respect to the middle plane of $Y = 0.5$. In Fig. 2(b), near the entrance, the velocity profile (curve A) is fairly uniform over the cross section. As the flow develops (curves B and C), the velocity in the core region is accelerated due to the entrance effect. Further downstream, the peak axial velocity moves toward the trailing wall ($X = 0$), as shown in curves E–G. This is clearly due to the onset of a second pair of counter-rotating vortices near the trailing wall [24, 25]. This second pair of vortices would push the peak axial velocity toward the trailing wall. In addition, it is found that the peak axial velocity becomes smaller from curve F to G. It is attributed to the Coriolis force induced by the secondary flow which is in the upstream direction in the core region [27]. It is also noted, in Fig. 2(b), that the axial velocity gradient on the trailing wall ($X = 0$) is larger than that on the leading wall ($X = 1$). This implies that the friction factor on the trailing wall is larger than that on the leading wall. Figure 2(a) gives the axial velocity profiles at $Y = 0.5$ with wall Reynolds number $Re_w = 10$. As before, curves A–C show the developing velocities in the entrance region. Moving away from the inlet, the effect of suction becomes more apparent. Further downstream, the peak axial velocity is smaller from curve E to G due to the combined effects of wall-transpiration and Coriolis force. The peak axial velocity is also shifted toward the porous wall (trailing wall) due to the outward suction force.

Figure 3 presents the axial variations of the circumferentially averaged friction factor fRe and Nusselt number, Nu, with wall Reynolds number, Re_w, as parameter. Figure 3(a) and (b) indicate that the suction effect is negligible up to a certain axial length Z.

Table 2. Comparisons of fanning friction factor of impermeable square duct

Z/Re	Shah and London [54]	This study
0.001	111.0	110.30
0.005	51.8	51.57
0.01	38.0	38.09
0.05	21.0	21.16
0.1	17.8	17.84

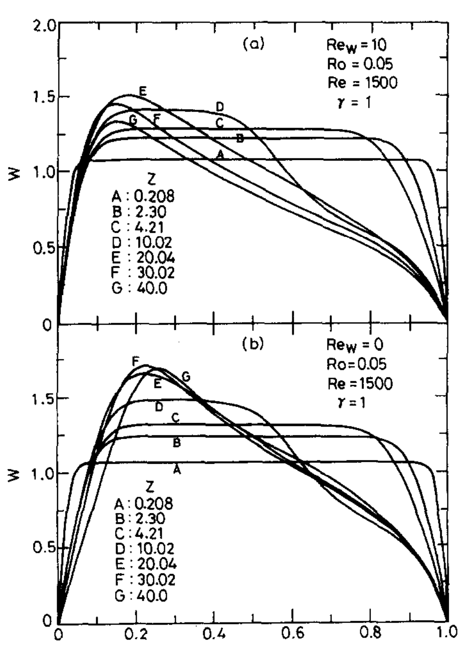

FIG. 2. Developments of axial velocity profiles at $Y = 0.5$.

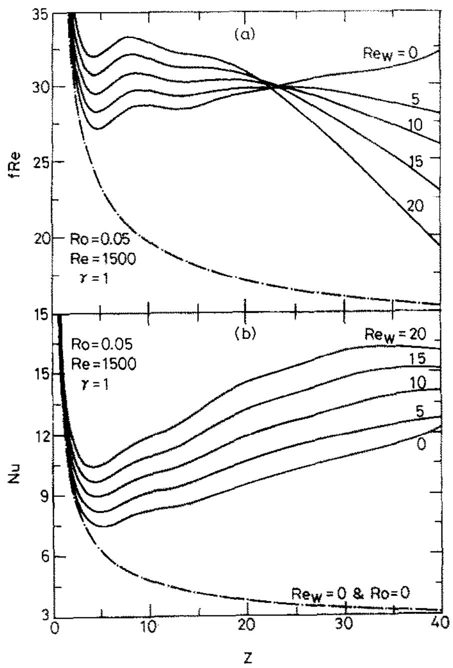

FIG. 3. Effects of Re_w on the variations of peripherally averaged friction factor and Nusselt number.

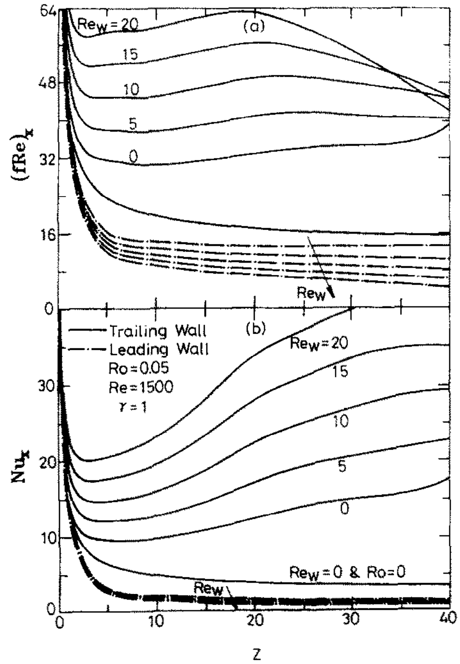

FIG. 4. Effects of Re_w on the variations of locally averaged friction factor and Nusselt number on the leading and trailing walls.

This axial distance depends primarily on the magnitude of the wall Reynolds number, Re_w. The greater Re_w is, the shorter the distance is. A further investigation reveals that the curves branch out from the purely forced convection results (i.e. $Re_w = 0$ and $Ro = 0$), and, after reaching a local minimum value, the curves increase. The occurrence of the first minimum in fRe or Nu is the appearance of the principal pair of vortices [25, 27]. In Fig. 3(a), the suction at the porous wall increases the fRe at the inlet section but decreases it further downstream. This is due to the fact that the wall transpiration attracts a large portion of the flowing mass to flow in a narrow region near the porous wall from which the fluid is being sucked. Therefore, the velocity gradient in this region increases, and, consequently, so does the fRe. However, as the flow proceeds in the axial direction, the total mass of the gas stream decreases due to the mass extraction, and hence the velocity gradient diminishes. This explains the reduction in the fRe in the downstream region. In Fig. 3(b), after the local minimum value, the Nu increases with the axial distance due to the effects of Coriolis force and wall suction. In addition, a larger Nu results for a larger Re_w. This is owing to the fact that wall suction changes the flow rate with the axial distance which has a hydrodynamic effect on the convective heat transfer. That is, the difference between heated wall temperature and bulk temperature is smaller for a larger wall suction, and hence the Nusselt number is larger for a higher Re_w.

The axial variations of locally averaged frictional factor $(fRe)_x$ and Nu_x on the trailing, leading and side walls are of interest. Figures 4 and 5 show the effects of the wall Reynolds number Re_w on the $(fRe)_x$ and Nu_x along the trailing, leading and side walls for $Ro = 0.05$, $Re = 1500$ and $\gamma = 1$. Near the entrance, the $(fRe)_x$ and $(Nu)_x$ on the leading wall fall steeply. As flow moves downstream, $(fRe)_x$ and Nu_x gradually decrease and level off. Furthermore, the larger $(fRe)_x$ and Nu_x result for a smaller Re_w on the leading wall. In contrast, the $(fRe)_x$ and Nu_x on the trailing wall vary significantly with Re_w. It is clear that, on the trailing wall, the larger $(fRe)_x$ and Nu_x are noted for a larger suction Reynolds number, Re_w, due to the suction effect along the trailing wall, except the result of $(fRe)_x$ for the case of $Re_w = 20$.

Figure 5 shows the locally averaged friction factor and heat transfer coefficient on the side walls. Comparing the results in Figs. 4 and 5 indicates that the $(fRe)_x$ and Nu_x on the side walls perform better than those on the leading wall but somewhat worse than those on the trailing wall. In Fig. 5(a), the $(fRe)_x$ on the side wall decreases with increasing suction Reynolds number, Re_w. In Fig. 5(b), near the entrance, the Nu_x increases with Re_w. But as the flow goes downstream, the trend is reversed.

The effects of rotation number, Ro, on the circumferentially averaged friction factor, fRe, and Nusselt number, Nu, are presented in Figs. 6(a) and (b), respectively. In these two plots, the rotation effects are negligible up to a certain distance depending mainly on the rotation number, Ro. The greater is Ro, the shorter is the distance. For each curve, a local minimum fRe or Nu is a result of the combined entrance and Coriolis effects. It is worth noting that

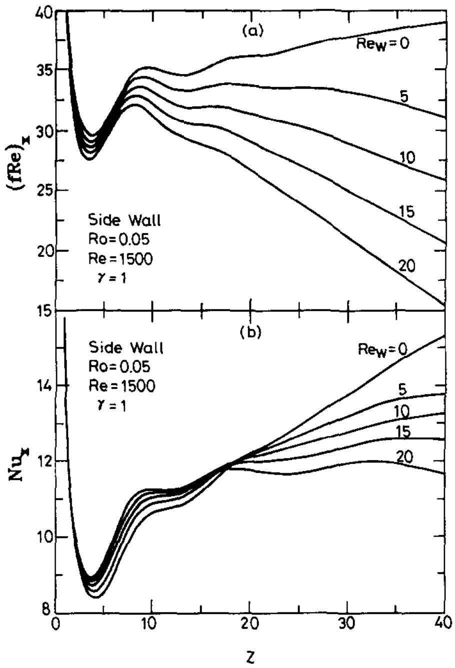

FIG. 5. Effects of Re_w on the variations of locally averaged friction factor and Nusselt number on the side walls.

for $Ro = 0.075$ and 0.1, oscillations in the variations of fRe and Nu exist after the first local minimum. This behavior is due to the emergence and decay of the second pair of vortices near the trailing wall. The similar trend is also found by Fann and Yang [25] for rotating heat transfer without wall-transpiration effects. In addition, the larger fRe and Nu result for a larger Ro due to the stronger Coriolis force.

Figure 7 shows the effect of the inlet Reynolds number, Re, on the variations of fRe and Nu for $Re_w = 10$, $Ro = 0.05$, and $\gamma = 1$. As shown in Fig. 7, larger fRe and Nu are experienced for a system with a higher inlet Reynolds number, Re, due to a larger forced-convection effect. It is also found in Fig. 7(a) that the fRe falls steeply with axial distance for $Re = 500$. This is because the suction effect is more significant for a system with a lower Re.

The effects of the channel aspect ratio, γ, on the friction factor fRe and Nusselt number Nu are of practical interest. The axial variations of fRe and Nu for aspect ratios $\gamma = 5$, 2, 0.5 and 0.2 are shown in Figs. 8 and 9, respectively, with wall Reynolds number, Re_w, as parameter. Comparing the results in Figs. 3, 8 and 9 indicates that wall suction effect is more pronounced for a system with a smaller γ. This is due to the fact that a channel with a smaller γ is a channel with a wider trailing wall (i.e. porous wall), which, in turn, causes a significant suction effect. Relatively, a larger fRe is noted for a system with a larger aspect ratio 5 ($\gamma = 2$) than that with $\gamma = 0.2$ ($\gamma = 0.5$), except the results near the entrance. This is owing to the fact that the relatively stronger secondary motion presented for aspect ratio $\gamma = 5$, which in turn causes a larger enhancement in fRe.

CONCLUSIONS

The characteristics of developing flow and heat transfer in radially rotating rectangular ducts with wall-transpiration effects have been studied numerically. A relatively novel vorticity–velocity method successively solved the 3-dimensional parabolic gov-

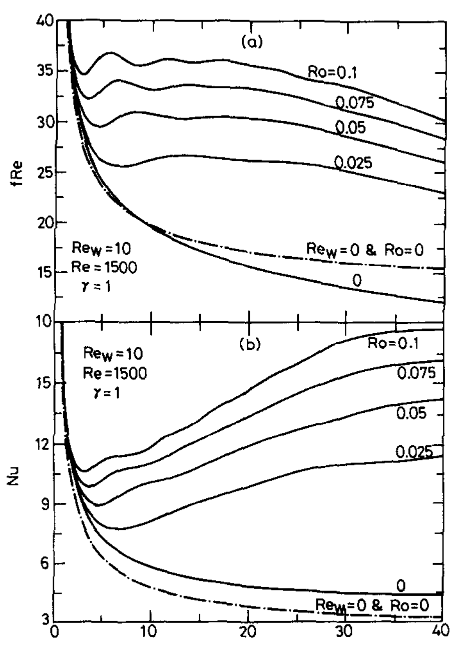

FIG. 6. The variations of the peripherally averaged friction factor and Nusselt number with Ro as parameter for $\gamma = 1$.

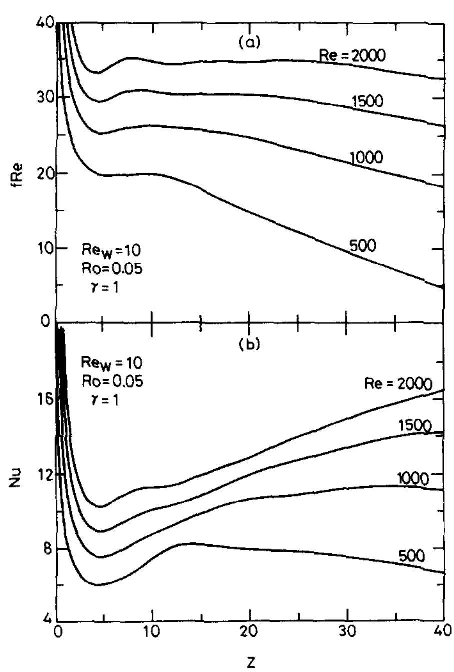

FIG. 7. Effects of Re on the variations of peripherally averaged friction factor and Nusselt number.

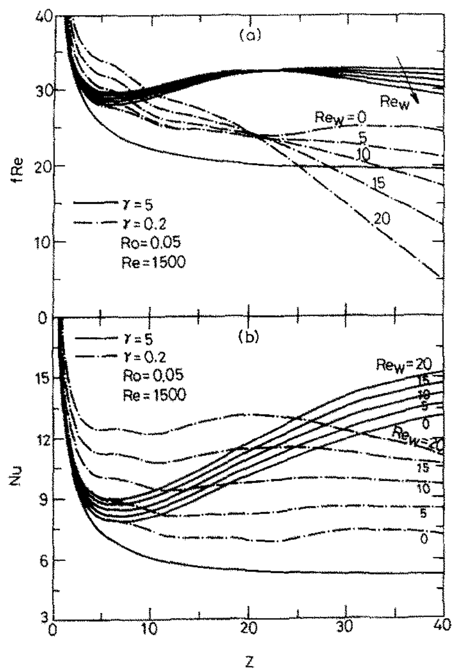

FIG. 8. The variations of the peripherally averaged friction factor and Nusselt number with Re_w as parameter for $\gamma = 5$ and 0.2.

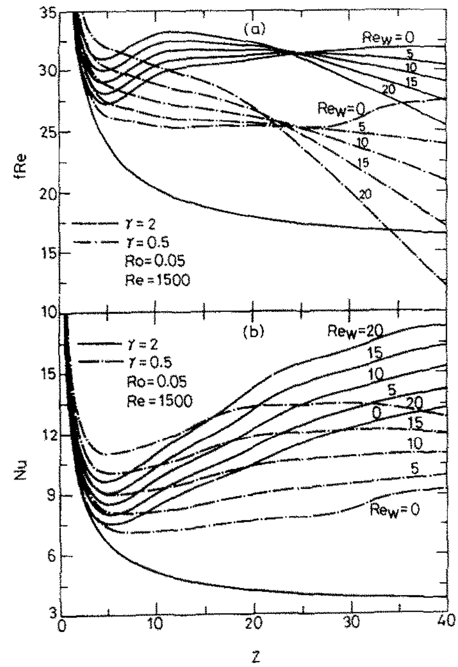

FIG. 9. The variations of the peripherally averaged friction factor and Nusselt number with Re_w as parameter for $\gamma = 2$ and 0.5.

erning equations. The effects of the wall Reynolds number, Re_w, rotation number, Ro, inlet Reynolds number, Re, and aspect ratio, γ, on the flow and heat transfer are examined in detail. What follows is a brief summary.

1. The variations of the friction factor, fRe, and Nusselt number, Nu, show that the effects of Coriolis force and wall-transpiration are negligible up to a certain entry length Z depending primarily on the magnitude of the rotation number, Ro, and wall Reynolds number, Re_w. The distributions of fRe and Nu are characterized by a decay near the entrance due to the entrance effect; but the decay is attenuated by the onset of secondary flow.
2. The circumferentially averaged Nusselt number, Nu, is enhanced with an increase in the wall Reynolds number, Re_w, rotation number, Ro, or inlet Reynolds number, Re.
3. Near the entrance, the fRe increases with Re_w. But as the flow moves downstream, the fRe decreases with Re_w.
4. The smaller suction effects on circumferentially averaged fRe and Nu are noted for a rectangular duct with a larger aspect ratio ($\gamma = 5$) due to the relatively narrower porous wall.

Acknowledgement—The financial support of this research by the National Science Council, R.O.C., under the contract NSC 82-0401-E211-016 is greatly appreciated.

REFERENCES

1. D. K. Hennecks, Heat transfer problems in aero-engines. In *Heat and Mass Transfer in Rotating Machinery* (Edited by D. E. Metzger and N. H. Afgan), pp. 353–379. Hemisphere, New York (1984).
2. C. Y. Soong, Transport phenomena in porous-walled ducts—a review, *Proceedings of the First National Conference on Science and Technology of National Defence*, Taiwan, R.O.C., pp. 241–249 (1992).
3. J. E. Hart, Instability and secondary flow in a rotating channel flow, *J. Fluid Mech.* **45**, 341–351 (1971).
4. H. Ito and K. Nanbu, Flow in rotating straight pipes of circular cross section, *J. Basic Engny* **93**, 383–394 (1971).
5. R. E. Wagner and H. R. Velkoff, Measurement of secondary flows in a rotating duct, *J. Engng Power* **94**, 261–270 (1972).
6. J. Moore, A wake and eddy in a rotating, radial-flow passage. Part 1: experimental observations, *J. Engng Power* **95**, 205–212 (1973).
7. J. Moore, A wake and eddy in a rotating, radial-flow passage. Part 2: flow model, *J. Engng Power* **95**, 213–219 (1973).
8. A. K. Majumdar and D. B. Spalding, A numerical investigation of three-dimensional flows in a rotating duct by a partially-parabolic procedure, HTS/76/26, Mech. Engng Dept., Imperial College of Science and Technology, London, U.K. (1976).
9. A. K. Majumdar, V. S. Pratap and D. B. Spalding, Numerical computation of flow in rotating ducts, *J. Fluid Engng* **99**, 148–153 (1977).
10. C. G. Speziale, Numerical study of viscous flow in rotating rectangular ducts, *J. Fluid Mech.* **122**, 251–271 (1982).
11. C. G. Speziale, Numerical solution of rotating internal flows, *Lec. Appl. Math.* **22**, 261–289 (1985).
12. C. G. Speziale and S. Thangam, Numerical study of secondary flows and roll-cell instabilities in rotating channel flow, *J. Fluid Mech.* **130**, 377–395 (1983).
13. Y. Mori, T. Fukada and W. Nakayama, Convective heat transfer in a rotating radial circular pipe (2nd Report), *Int. J. Heat Mass Transfer* **11**, 1807–1824 (1971).
14. V. Vidyanidhi, V. V. S. Suryanarayana and R. Chenchu, An analysis of steady fully developed heat transfer in

a rotating straight pipe, *J. Heat Transfer* **99**, 148–153 (1977).
15. D. E. Metzger and R. L. Stan, Entry region heat transfer in rotating radial tubes, AIAA Paper No. 77-189, presented at the 15th AIAA Aerospace Sciences Meeting, Los Angeles, CA (1977).
16. W. D. Morris and T. Ayhan, Observation on the influence of rotation on heat transfer in the coolant channel of gas turbine rotor blade, *Proc. Inst. Mech. Engrs* **193**, 303–311 (1979).
17. W. D. Morris and T. Ayhan, An experimental study of turbulent heat transfer in the tube which rotates about an orthogonal axis, *Proc. XIV ICHMT Symposium on Heat and Mass Transfer in Rotating Machinery*, Dubrovnik, Yugoslavia, 30 August–3 September (1982).
18. R. J. Clifford, S. P. Harasgama and W. D. Morris, An experimental study of local and mean heat transfer in a triangular-sectional duct rotating in the orthogonal mode, *J. Engng Gas Turbines Power* **106**, 661–667 (1984).
19. G. J. Hwang and C. Y. Soong, Experimental automation and heat transfer measurement on a rotating thermal system. In *Transport Phenomena in Thermal Control* (Edited by G. J. Hwang), pp. 375–388. Hemisphere, New York (1989).
20. G. J. Hwang and T. C. Jen, Convective heat transfer in rotating isothermal ducts, *Int. J. Heat Mass Transfer* **33**, 1817–1828 (1990).
21. J. H. Wagner, B. V. Johnson and T. J. Hajek, Heat transfer in rotating passages with square smooth walls and radial outward flow, *J. Turbomach.* **113**, 42–51 (1991).
22. J. H. Wanger, B. V. Johnson and F. C. Kopper, Heat transfer in rotating serpentine passage with smooth walls, *J. Turbomach.* **113**, 321–330 (1991).
23. C. Y. Soong, S. T. Lin and G. J. Hwang, An experimental study of convective heat transfer in radially rotating rectangular ducts, *J. Heat Transfer* **113**, 604–611 (1991).
24. S. Fann, W. J. Yang and S. Mochizuki, Transport phenomena in laminar developing flow of rotating heated channels, *4th Symp. on Transport Phenomena and Dynamics of Rotating Machinery*, Vol. B, pp. 511–525 (1992).
25. S. Fann and W. J. Yang, Hydrodynamically and thermally developing laminar flow through rotating channel having isothermal walls, *Numer. Heat Transfer* **22**, Part A, 257–288 (1992).
26. J. C. Han and Y. M. Zhang, Effect of uneven wall temperature on local heat transfer in a rotating square channel with smooth walls and radial outward flow, *J. Heat Transfer* **114**, 850–858 (1992).
27. T. C. Jen, A. S. Lavine and G. J. Hwang, Simultaneously developing laminar convection in rotating isothermal square channels, *Int. J. Heat Mass Transfer* **35**, 239–254 (1992).
28. T. C. Jen and A. S. Lavine, Laminar heat transfer and fluid flow in the entrance region of a rotating duct with rectangular cross section: the effect of aspect ratio, *J. Heat Transfer* **114**, 574–581 (1992).
29. W. E. Wageman and F. A. Guevana, Fluid flow through a porous channel, *Phys. Fluids* **3**, 878–881 (1960).
30. R. W. Hornbeck, W. T. Rouleau and F. Osterle, Laminar entry problem in porous tubes, *Phys. Fluids* **6**, 1649–1654 (1963).
31. S. Prager, Spiral flow in a stationary porous pipe, *Phys. Fluids* **7**, 907–908 (1964).
32. R. M. Terrill and P. W. Thomas, Spiral flow in a porous pipe, *Phys. Fluids* **16**, 356–359 (1973).
33. R. M. Terril, An exact solution for flow in a porous pipe, *J. Appl. Math. Phys.* **33**, 547–552 (1982).
34. R. M. Terrill, Laminar flow in a porous tube, *J. Fluid Engng* **105**, 303–307 (1983).
35. I. E. Idel'chik and M. O. Shteinberg, Total pressure losses in porous cylindrical tubes with a path-dependent flowrate, *Thermal Engng* **35**, 52–55 (1988).
36. G. D. Raithby and D. C. Knudsen, Hydrodynamic development in a duct with suction and blowing, *J. Appl. Mech.* **41**, 896–902 (1974).
37. M. M. Sorour, M. A. Hassab and S. Estafanous, Developing laminar flow in a semiporous two-dimensional channel with nonuniform transpiration, *Int. J. Heat Fluid Flow* **8**, 44–54 (1987).
38. M. K. Tasi and T. M. Liou, Fiber optic LDV study of the nonuniform injection-induced flow in a 2-D, divergent porous-walled channel, *J. Chinese Soc. Mech. Engng* **11**, 414–422 (1991).
39. M. K. Tsai and T. M. Liou, Study of flow induced by nonuniform lateral injection, *J. Propulsion Power* **7**, 668–677 (1991).
40. L. F. Carter and W. N. Gill, Asymptotic solution for combined free and forced convection in vertical and horizontal conduits with uniform suction and blowing, *A.I.Ch.E. Jl* **10**, 330–339 (1964).
41. R. B. Kinney, Fully developed frictional and heat transfer characteristics of laminar flow in porous tubes, *Int. J. Heat Mass Transfer* **11**, 1393–1401 (1968).
42. R. J. Pederson and R. B. Kinney, Entrance-region heat transfer for laminar flow in porous tubes, *Int. J. Heat Mass Transfer* **14**, 159–161 (1971).
43. G. D. Raithby, Laminar heat transfer in the thermal entrance region of circular tubes and two-dimensional rectangular ducts with wall suction and injection, *Int. J. Heat Mass Transfer* **14**, 224–243 (1971).
44. J. R. Doughty and H. C. Perkins, Jr., Thermal and combined entry problems for laminar flow between parallel porous plates, *J. Heat Transfer* **94**, 233–234 (1972).
45. J. R. Doughty and H. C. Perkins, Jr., Variable properties laminar gas flow heat transfer in the entry region of parallel porous plates, *Int. J. Heat Mass Transfer* **16**, 663–668 (1973).
46. S. J. Rhee and D. K. Edwards, Laminar entrance flow in a flat plate duct with asymmetric suction and heating, *Numer. Heat Transfer* **4**, 85–100 (1981).
47. A. Fagher, Heat-transfer characteristics in annuli with blowing or suction at the walls, *J. Thermophys. Heat Transfer* **4**, 59–66 (1990).
48. C. Y. Soong and G. J. Hwang, Laminar mixed convection in a radially rotating semiporous channel, *Int. J. Heat Mass Transfer* **33**, 1805–1816 (1990).
49. C. Y. Soong and G. J. Hwang, Effects of stress work on similarity solutions of mixed convection in rotating channel with wall-transpiration, *Int. J. Heat Mass Transfer* **36**, 845–856 (1993).
50. S. V. Patankar and D. B. Spalding, A calculation procedure for heat, mass and momentum transfer in three-dimensional parabolic flows, *Int. J. Heat Mass Transfer* **15**, 1787–1806 (1972).
51. K. Ramakrishna, S. G. Rubin and P. K. Khosla, Laminar natural convection along vertical square ducts, *Numer. Heat Transfer* **5**, 59–79 (1982).
52. P. J. Roache, *Computational Fluid Dynamics*, pp. 61–64. Reinhold, New York (1971).
53. F. C. Chou and G. J. Hwang, Vorticity–velocity method for Graetz problem with the effect of natural convection in a horizontal rectangular channel with uniform wall heat flux, *J. Heat Transfer* **109**, 704–710 (1987).
54. R. A. Shah and A. L. London, Laminar flow forced convection in ducts, Suppl. 1 to *Adv. Heat Transfer*, pp. 196–222. Academic Press, New York (1978).